Fluid Dynamics of Free Convection Flow in Unsteady State over Single Inclined Flat Plate

Mohammad Ghani, Tri Utomo, Yolanda Norasia, Denis Sospeter Mukama

***Abstract*—Being motivated by the previous studies, we consider the concentration, the natural convection of fluid flow, and the inclination angle in this paper where the mathematical model is solved numerically by using the Crank-Nicolson scheme. At the first stage, the finite difference approximation are applied into the non-dimensional governing equations. As we know that the implicit finite difference method cannot be iterated directly, we need the strategy by taking an iteration through the Thomas algorithm, where this algorithm can be applied to solve the tri-diagonal matrices iteratively.**

Using the software, we further provide the simulations of velocity, temperature, and concentration profiles of fluid flow over an inclined flat plate based on the results of finite-difference approximations to non-dimensional governing equations. Finally, we use the general term of Fourier expansion to establish the stability of the finite difference scheme.

***Index Terms*—Thermal Boundary Layer; Grashof number (G_r); Modified Grashof number (G_m); Prandtl number (P_r); Schmidt number (S_c).**

I. Introduction

RESEARCHERS have studied numerical simulations of convection flow through a flat plate extensively, and they are widely used in engineering applications. Many researchers have been interested in flow of mixed convection with Newtonian or non-Newtonian fluids in various geometries such as spheres, cones, and cylinders. The steady-incompressible flow of mixed convection over single solid sphere medium was investigated and solved numerically under the constant temperature [1]. The Keller-Box method was used to solve the numerical solutions for the mixed convection flow over a sphere with Newtonian heating in [15]. The local surface temperature increased in direct proportion to the Newtonian heating. Kasim [9] wanted to investigate the steady-incompressible flow mixed convection under viscoelastic fluid through a solid sphere using the Keller-Box. The Crank-Nicolson and iterative methods was used to compute numerical results of steady-incompressible flow of mixed convection over single sphere [4]. The aspects of magnetohydrodynamics (MHD) was extensively studied in [5] using the Keller-Box method, which was based on the previous mathematical model. Widodo et al. [19] investigated the non-steady state of MHD model over single solid sphere under the effect of a micro-polar fluid. Recently, the heat, slip flow, and thermal radiation of ferrofluid have been extensively studied in [10], [21], [8], [13], [20], [3], [11] for several medium. Ferrofluid is used in the cooling systems of electronic devices such as hard disks of computer in the industrial sector. The ferrofluid has been used in medical applications such as cancer therapy [17]. The ferrofluid potential in medicine is difficult to investigate, especially when blood is used as the base fluid. Because its properties differ from those of a Newtonian fluid such as water, blood is classified as a non-Newtonian type fluid. The non-Newtonian fluid model's properties were not represented in the standard Navier-Stokes equations. The Navier-Stokes equations in [12] must then be adjusted to account for the non-Newtonian type fluid. To recognize the elastic or solid-fluid behavior, the Casson problem is classified as non-Newtonian type fluid. Daniel et al. [2] used various graphical and tabular forms to investigate the effect of the electric field, thermal radiation, viscous dissipation, and chemical reaction on nanofluid flow and heat transfer. The entropy generation of MHD Couette flow through a vertical microchannel was investigated in [16] while taking Ion slip into account. Meanwhile, Nayak [14] investigated MHD flow and heat transfer of third grade through two long parallel flat porous plates, and the damped-Newton method has been employed to provide the numerical aspects. Salah et al. investigated accelerated MHD flow of second grade through a porous medium and rotating frame in [18]. Based on previous work, we investigate the numerical aspects of natural convection flow over single inclined flat plate using the numerical scheme of Crank-Nicolson scheme, where the approximations results of systems are then iteratively solved by the Thomas algorithm. Moreover, this paper is the combination of the studies in [6] and [7], where the inclination of the single flat plate is considered under the effect of the natural convection of fluid flow. The numerical solution is provided by applying the numerical scheme of Crank-Nicolson, where this method has the stability characteristic unconditionally stable under the Fourier expansion technique.

Other parts of this work are organized in the following aspects. The Section 2 points the physical model of fluid flow over single inclined flat plate α. Then, the approximations of Eqs. (7)-(10) and the numerical simulations are presented in the Section 3. The stability analysis is presented in Section 4 by conducting the appropriate general form of Fourier expansion, to provide the stability aspect of finite difference of numerical scheme. The summaries of the effect the Grashof number (G_r), Modified Grashof number (G_m), Prandtl number (P_r), Schmidt number (S_c) to unsteady free convection flow over an inclined flat plate and also the stability results are established in Section 5.

Manuscript received November 07, 2022; revised March 08, 2023. This work was supported by Faculty of Advanced Technology and Multidiscipline, Universitas Airlangga, Indonesia under the contract number 121/UN3.1.17/PT/2022.

Mohammad Ghani is a Lecturer in the Technology of Data Science, Faculty of Advanced Technology and Multidiscipline, Universitas Airlangga, Indonesia (Corresponding author, email: mohammad.ghani@ftmm.unair.ac.id)

Tri Utomo is a Lecturer in the Department of Mathematics, Institut Teknologi Sumatera, Indonesia (email: three1st@gmail.com)

Yolanda Norasia is a Lecturer in the Department of Mathematics, UIN Walisongo, Indonesia (email: yolandanorasia@walisongo.ac.id)

Denis Sospeter Mukama is a Lecturer in the Dar es Salaam University College of Education, University of Dar es Salaam, Tanzania (email: dmukama86@gmail.com)

II. Mathematical Model

The X-axis is vertically along the inclined flat plate related to the flow direction, and the Y-axis is related to the normal of an inclined flat plate in the Cartesian coordinate. In this research, we consider that the temperature between the inclined flat plate (T) and fluid (T_∞) are same, and the concentration for both inclined flat plate (C) and fluid (C_∞) are also same. The velocity of fluid over the inclined flat plate will change for all the time $t > 0$, with the distinct values of the Grashof number (G_r), Modified Grashof number (G_m), Prandtl number (P_r), Schmidt number (S_c). The concentration and temperature are respectively represented by C_w and T_w at the wall of the inclined flat plate. The concentration and temperature of the fluid in the environment (near the inclined flat plate) are respectively represented by C_∞ and T_∞. In this paper, the physical model of fluid flow over an inclined flat plate α refers to the Figure 1.

According to Figure 1, the phenomena of fluid flow over single inclined flat plate is presented in the following coupled dimensional systems, where this can be obtained from the continuity, momentum, energy, and concentration equations respectively:

$$\frac{\partial u}{\partial x} + \frac{\partial v}{\partial y} = 0, \tag{1}$$

$$\begin{aligned}\frac{\partial u}{\partial t} + u\frac{\partial u}{\partial x} + v\frac{\partial u}{\partial y} = \nu\frac{\partial^2 u}{\partial y^2} + g\beta(T - T_\infty)sin(\alpha) \\ + g\beta^*(C - C_\infty),\end{aligned} \tag{2}$$

$$\frac{\partial T}{\partial t} + u\frac{\partial T}{\partial x} + v\frac{\partial T}{\partial y} = \frac{K}{\rho C_p}\frac{\partial^2 T}{\partial y^2} + Q(T_\infty - T), \tag{3}$$

$$\frac{\partial C}{\partial t} + u\frac{\partial C}{\partial x} + v\frac{\partial C}{\partial y} = D\frac{\partial^2 C}{\partial y^2}. \tag{4}$$

Moreover, the initial and boundary values are given below,

$$\begin{aligned}&\text{at } t = 0\\ &\quad u = 0,\ v = 0,\ T \to T_\infty,\ C \to C_\infty, \text{ everywhere},\\ &\text{at } t > 0\\ &\quad u = 0,\ v = 0,\ T \to T_\infty,\ C \to C_\infty, \text{ at } x = 0,\\ &\quad u = 0,\ v = 0,\ T \to T_w,\ C \to C_w, \text{ at } y = 0,\\ &\quad u = 0,\ v = 0,\ T \to T_w,\ C \to C_w, \text{ as } y \to \infty.\end{aligned} \tag{5}$$

where x, y refers to the cartesian coordinate of systems. Moreover, u, v represents the fluid velocity in the axes x, y, where local acceleration is affected by the gravity, the kinematic viscosity ν, the density of the fluid ρ, thermal conductivity K, the specific heat for constant pressure C_p, and the coefficient of mass diffusivity D.

Our goal is to establish the implicit finite difference method of Crank-Nicolson to the governing equations (1)-(4) with the initial and boundary values in (5), then it is required to change the dimensional to be the non-dimensional systems. Because of this purpose, then we present Eq. (6),

$$\begin{aligned}&X = \frac{xU_0}{\nu},\ Y = \frac{yU_0}{\nu},\ U = \frac{u}{U_0},\ V = \frac{v}{U_0},\ \xi = \frac{tU_0^2}{\nu},\\ &\bar{W} = \frac{T - T_\infty}{T_w - T_\infty},\ \bar{R} = \frac{C - C_\infty}{C_w - C_\infty}.\end{aligned} \tag{6}$$

Then, the following non-dimensional systems are obtained based on Eq. (6) and Eqs. (1)-(4),

$$\frac{U_0^2}{\nu}\left(\frac{\partial U}{\partial X} + \frac{\partial V}{\partial Y}\right) = 0,$$

$$\begin{aligned}&\frac{U_0^3}{\nu}\left(\frac{\partial U}{\partial \xi} + U\frac{\partial U}{\partial X} + V\frac{\partial U}{\partial Y}\right)\\ &= \frac{U_0^3}{\nu}\frac{\partial^2 U}{\partial Y^2} + Gr(T_w - T_\infty)\bar{W}sin(\alpha) + G_m(C_w - C_\infty)\bar{R},\end{aligned}$$

$$\begin{aligned}&\frac{(T_w - T_\infty)U_0^2}{\nu}\left(\frac{\partial \bar{W}}{\partial \xi} + U\frac{\partial \bar{W}}{\partial X} + V\frac{\partial \bar{W}}{\partial Y}\right)\\ &= \frac{kU_0^2(T_w - T_\infty)}{\rho C_p \nu^2}\frac{\partial^2 \bar{W}}{\partial Y^2} - Q\bar{W}(T_w - T_\infty),\end{aligned}$$

$$\begin{aligned}&\frac{(C_w - C_\infty)U_0^2}{\nu}\left(\frac{\partial \bar{R}}{\partial \xi} + U\frac{\partial \bar{R}}{\partial X} + V\frac{\partial \bar{R}}{\partial Y}\right)\\ &= \frac{DU_0^2(C_w - C_\infty)}{\nu^2}\frac{\partial^2 \bar{R}}{\partial Y^2},\end{aligned}$$

Then, we finally simplify the above results, one has

$$\frac{\partial U}{\partial X} + \frac{\partial V}{\partial Y} = 0, \tag{7}$$

$$\frac{\partial U}{\partial \xi} + U\frac{\partial U}{\partial X} + V\frac{\partial U}{\partial Y} = \frac{\partial^2 U}{\partial Y^2} + Gr\bar{W}sin(\alpha) + G_m\bar{R}, \tag{8}$$

$$\frac{\partial \bar{W}}{\partial \xi} + U\frac{\partial \bar{W}}{\partial X} + V\frac{\partial \bar{W}}{\partial Y} = \frac{1}{P_r}\frac{\partial^2 \bar{W}}{\partial Y^2} - \phi\bar{W}, \tag{9}$$

$$\frac{\partial \bar{R}}{\partial \xi} + U\frac{\partial \bar{R}}{\partial X} + V\frac{\partial \bar{R}}{\partial Y} = \frac{1}{S_c}\frac{\partial^2 \bar{R}}{\partial Y^2}, \tag{10}$$

where the non-dimensional variables are given below,

$$\begin{aligned}&\text{Grashof number:}\\ &\qquad G_r = \nu g\beta\frac{T_w - T_\infty}{U_0^3}.\\ &\text{Modified Grashof number:}\\ &\qquad G_m = \nu g\beta^*\frac{C_w - C_\infty}{U_0^3}.\\ &\text{Prandtl number:}\\ &\qquad P_r = \frac{\nu\rho C_p}{K}.\\ &\text{Schmidt number:}\\ &\qquad S_c = \frac{\nu}{D}.\\ &\text{Heat source:}\\ &\qquad \phi = \frac{Q\nu}{U_0^2}.\end{aligned} \tag{11}$$

Moreover, the initial and boundary variables are presented below,

$$\begin{aligned}&\text{at } \xi = 0\\ &\quad U = 0,\ V = 0,\ \bar{W} = 0,\ \bar{R} = 0 \text{ everywhere},\\ &\text{at } \xi > 0\\ &\quad U = 0,\ V = 0,\ \bar{W} = 0,\ \bar{R} = 0, \text{ at } X = 0,\\ &\quad U = 0,\ V = 0,\ \bar{W} = 1,\ \bar{R} = 1, \text{ at } Y = 0,\\ &\quad U = 0,\ V = 0,\ \bar{W} = 0,\ \bar{R} = 0, \text{ as } Y \to \infty.\end{aligned} \tag{12}$$

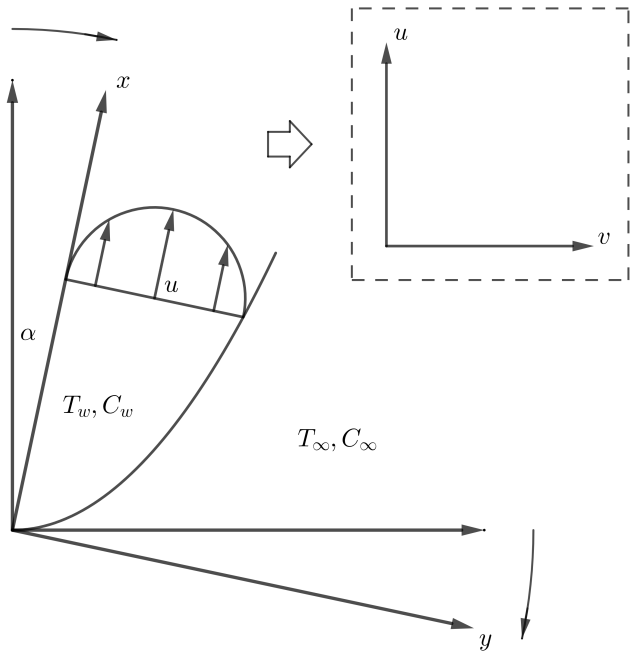

Fig. 1. The physical model of an inclined flat plate

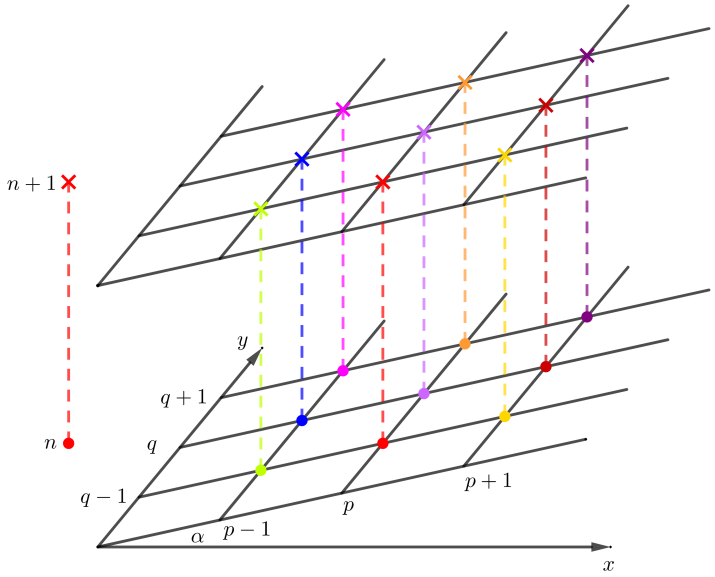

Fig. 2. The finite difference space grid with inclination angle α

III. Numerical Analysis

We are devoted to studying the non-dimensional systems in the second order of coupled differential equations subject to the initial and boundary values. The analytical solution of our system is near impossible to be provided, then we approximate the non-dimensional systems by using finite difference of numerical scheme. For the numerical aspect, we apply the implicit numerical scheme of Crank-Nicolson. This Crank-Nicolson method is applied to the systems (7)-(10) under the initial and boundary values in (12). Then, the fluid flow direction is assumed as the parallel grid of lines towards X-axis and Y-axis. This aims is to provide the numerical scheme of (7)-(10), where X-axis is vertically along with an inclined plate and Y-axis is normal to the plate. The notations U^{n+1}, V^{n+1}, T^{n+1}, C^{n+1} represent the values of U, V, $\bar{W}$, $\bar{R}$ respectively at the next step of time.

Numerical approximations for second-order derivative

$$\left(\frac{\partial^2 U}{\partial Y^2}\right)_{p,q} = \frac{U_{p,q+1} - 2U_{p,q} + U_{p,q-1}}{(\Delta Y)^2},$$
$$\left(\frac{\partial^2 \bar{W}}{\partial Y^2}\right)_{p,q} = \frac{\bar{W}_{p,q+1} - 2\bar{W}_{p,q} + \bar{W}_{p,q-1}}{(\Delta Y)^2}, \qquad (13)$$
$$\left(\frac{\partial^2 \bar{R}}{\partial Y^2}\right)_{p,q} = \frac{\bar{R}_{p,q+1} - 2\bar{R}_{p,q} + \bar{R}_{p,q-1}}{(\Delta Y)^2}.$$

Numerical approximations for first-order derivative

$$\begin{aligned}
&\left(\frac{\partial U}{\partial \xi}\right)_{p,q}=\frac{U_{p,q}^{n+1}-U_{p,q}^{n}}{\Delta \xi},\left(\frac{\partial \bar{W}}{\partial \xi}\right)_{p,q}=\frac{\bar{W}_{p,q}^{n+1}-\bar{W}_{p,q}^{n}}{\Delta \xi},\\
&\left(\frac{\partial U}{\partial Y}\right)_{p,q}=\frac{U_{p,q}-U_{p,q-1}}{\Delta Y},\left(\frac{\partial V}{\partial Y}\right)_{p,q}=\frac{V_{p,q}-V_{p,q-1}}{\Delta Y},\\
&\left(\frac{\partial T}{\partial Y}\right)_{p,q}=\frac{\bar{W}_{p,q}-\bar{W}_{p,q-1}}{\Delta Y},\left(\frac{\partial U}{\partial Y}\right)_{p,q}=\frac{U_{p,q+1}-U_{p,q-1}}{2\Delta Y},\\
&\left(\frac{\partial V}{\partial Y}\right)_{p,q}=\frac{V_{p,q+1}-V_{p,q-1}}{2\Delta Y},\left(\frac{\partial \bar{W}}{\partial Y}\right)_{p,q}=\frac{\bar{W}_{p,q+1}-\bar{W}_{p,q-1}}{2\Delta Y},\\
&\left(\frac{\partial U}{\partial X}\right)_{p,q}=\frac{U_{p,q}-U_{p-1,q}}{\Delta X},\left(\frac{\partial V}{\partial X}\right)_{p,q}=\frac{V_{p,q}-V_{p-1,q}}{\Delta X},\\
&\left(\frac{\partial \bar{W}}{\partial X}\right)_{p,q}=\frac{\bar{W}_{p,q}-\bar{W}_{p-1,q}}{\Delta X},\left(\frac{\partial \bar{R}}{\partial \xi}\right)_{p,q}=\frac{\bar{R}_{p,q}^{n+1}-\bar{R}_{p-1,q}^{n}}{\Delta \xi},\\
&\left(\frac{\partial \bar{R}}{\partial Y}\right)_{p,q}=\frac{\bar{R}_{p,q}-\bar{R}_{p,q-1}}{\Delta Y},\left(\frac{\partial \bar{R}}{\partial Y}\right)_{p,q}=\frac{\bar{R}_{p,q+1}-\bar{R}_{p,q-1}}{2\Delta Y},\\
&\left(\frac{\partial \bar{R}}{\partial X}\right)_{p,q}=\frac{\bar{R}_{p,q}-\bar{R}_{p-1,q}}{\Delta X},
\end{aligned} \tag{14}$$

where the subscripts p and q represent the X-axis and Y-axis, the superscript n provides the time variable of ξ. The finite difference of numerical scheme can be represented in Figure 2, where ΔX and ΔY respectively represent the step size in X-axis and Y-axis. By substituting the previous results of numerical scheme into Eqs. (7)-(10), the appropriate numerical scheme is given below,

$$\begin{aligned}
&\frac{1}{\Delta \xi}\left(U_{p,q}^{n+1}-U_{p,q}^{n}\right)\\
&+\frac{U_{p,q}^{n}}{2\Delta X}\left(U_{p,q}^{n+1}-U_{p-1,q}^{n+1}+U_{p,q}^{n}-U_{p-1,q}^{n}\right)\\
&+\frac{V_{p,q}^{n}}{4\Delta Y}\left(U_{p,q+1}^{n+1}-U_{p,q-1}^{n+1}+U_{p,q+1}^{n}-U_{p,q-1}^{n}\right)=\\
&\frac{1}{2(\Delta Y)^{2}}\left(U_{p,q-1}^{n+1}-2U_{p,q}^{n+1}+U_{p,q+1}^{n+1}\right)\\
&\frac{1}{2(\Delta Y)^{2}}\left(U_{p,q+1}^{n+1}+U_{p,q-1}^{n}-2U_{p,q}^{n}+U_{p,q+1}^{n}\right)\\
&+G_{r}\frac{\bar{W}_{p,q}^{n+1}+\bar{W}_{p,q}^{n+1}}{2}sin(\alpha)+G_{m}\frac{\bar{R}_{p,q}^{n+1}+\bar{R}_{p,q}^{n+1}}{2}.
\end{aligned} \tag{15}$$

$$\begin{aligned}
&\frac{1}{\Delta \xi}\left(\bar{W}_{p,q}^{n+1}-\bar{W}_{p,q}^{n}\right)\\
&+\frac{U_{p,q}^{n}}{2\Delta X}\left(\bar{W}_{p,q}^{n+1}-\bar{W}_{p-1,q}^{n+1}+\bar{W}_{p,q}^{n}-\bar{W}_{p-1,q}^{n}\right)+\\
&\frac{V_{p,q}^{n}}{4\Delta Y}\left(\bar{W}_{p,q+1}^{n+1}-\bar{W}_{p,q-1}^{n+1}+\bar{W}_{p,q+1}^{n}-\bar{W}_{p,q-1}^{n}\right)=\\
&\frac{1}{2P_{r}(\Delta Y)^{2}}\left(\bar{W}_{p,q-1}^{n+1}-2\bar{W}_{p,q}^{n+1}+\bar{W}_{p,q+1}^{n+1}\right)\\
&\frac{1}{2P_{r}(\Delta Y)^{2}}\left(\bar{W}_{p,q-1}^{n}-2\bar{W}_{p,q}^{n}+\bar{W}_{p,q+1}^{n}\right)\\
&-\phi\frac{\bar{W}_{p,q}^{n+1}+\bar{W}_{p,q}^{n}}{2}.
\end{aligned} \tag{16}$$

$$\begin{aligned}
&\frac{1}{\Delta \xi}\left(\bar{R}_{p,q}^{n+1}-\bar{R}_{p,q}^{n}\right)\\
&+\frac{U_{p,q}^{n}}{2\Delta X}\left(\bar{R}_{p,q}^{n+1}-\bar{R}_{p-1,q}^{n+1}+\bar{R}_{p,q}^{n}-\bar{R}_{p-1,q}^{n}\right)+\\
&\frac{V_{p,q}^{n}}{4\Delta Y}\left(\bar{R}_{p,q+1}^{n+1}-\bar{R}_{p,q-1}^{n+1}+\bar{R}_{p,q+1}^{n}-\bar{R}_{p,q-1}^{n}\right)=\\
&\frac{1}{2S_{c}(\Delta Y)^{2}}\left(\bar{R}_{p,q-1}^{n+1}-2\bar{R}_{p,q}^{n+1}+\bar{R}_{p,q+1}^{n+1}\right)\\
&\frac{1}{2S_{c}(\Delta Y)^{2}}\left(\bar{R}_{p,q-1}^{n}-2\bar{R}_{p,q}^{n}+\bar{R}_{p,q+1}^{n}\right).
\end{aligned} \tag{17}$$

$$\begin{aligned}
&\frac{1}{2\Delta X}\left(U_{p,q}^{n+1}-U_{p-1,q}^{n+1}+U_{p,q}^{n}-U_{p-1,q}^{n}\right)\\
&+\frac{1}{2\Delta X}\left(U_{p,q-1}^{n+1}-U_{p-1,q-1}^{n+1}+U_{p,q-1}^{n}-U_{p-1,q-1}^{n}\right)\\
&+\frac{1}{\Delta Y}\left(V_{p,q}^{n+1}-V_{p,q-1}^{n+1}+V_{p,q}^{n}-V_{p,q-1}^{n}\right)=0.
\end{aligned} \tag{18}$$

We arrange the finite-difference results (18)-(17) into the same term of time $n+1$ and n, and then one has the following finite difference approximations,

$$\begin{aligned}
V_{p,q}^{n+1}=&V_{p,q-1}^{n+1}-V_{p,q}^{n}+V_{p,q-1}^{n}-\\
&C_{1}\begin{pmatrix}U_{p,q}^{n+1}-U_{p-1,q}^{n+1}+U_{p,q}^{n}-U_{p-1,q}^{n}+\\ U_{p,q-1}^{n+1}-U_{p-1,q-1}^{n+1}+U_{p,q-1}^{n}-U_{p-1,q-1}^{n}\end{pmatrix},
\end{aligned} \tag{19}$$

$$\begin{aligned}
&(-C_{2}-C_{3})U_{p,q-1}^{n+1}+(1+C_{4}+2C_{3})U_{p,q}^{n+1}+\\
&(C_{2}-C_{3})U_{p,q+1}^{n+1}=U_{p,q}^{n}+C_{4}(U_{p-1,q}^{n+1}+U_{p-1,q}^{n}-U_{p,q}^{n})\\
&\qquad+C_{2}(U_{p,q-1}^{n}-U_{p,q+1}^{n})\\
&\qquad+C_{3}(U_{p,q-1}^{n}-2U_{p,q}^{n}+U_{p,q+1}^{n})\\
&\qquad+C_{5}(\bar{W}_{p,q}^{n+1}+\bar{W}_{p,q}^{n})\\
&\qquad+C_{6}(\bar{R}_{p,q}^{n+1}+\bar{R}_{p,q}^{n}),
\end{aligned} \tag{20}$$

$$\begin{aligned}
&(-C_{7}-C_{8})\bar{W}_{p,q-1}^{n+1}+(1+C_{9}+2C_{8}+C_{10})\bar{W}_{p,q}^{n+1}+\\
&(C_{7}-C_{8})\bar{W}_{p,q+1}^{n+1}=(1-C_{11})\bar{W}_{p,q}^{n}\\
&\qquad+C_{9}(\bar{W}_{p-1,q}^{n+1}+\bar{W}_{p-1,q}^{n}-\bar{W}_{p,q}^{n})\\
&\qquad+C_{7}(\bar{W}_{p,q-1}^{n}-\bar{W}_{p,q+1}^{n})\\
&\qquad+C_{8}(\bar{W}_{p,q-1}^{n}-2\bar{W}_{p,q}^{n}+\bar{W}_{p,q+1}^{n}),
\end{aligned} \tag{21}$$

$$\begin{aligned}
&(-C_{12}-C_{13})\bar{R}_{p,q-1}^{n+1}+(1+C_{14}+2C_{13})\bar{W}_{p,q}^{n+1}+\\
&(C_{12}-C_{13})\bar{R}_{p,q+1}^{n+1}=\bar{R}_{p,q}^{n}\\
&\qquad+C_{14}(\bar{R}_{p-1,q}^{n+1}+\bar{R}_{p-1,q}^{n}-\bar{R}_{p,q}^{n})\\
&\qquad+C_{12}(\bar{R}_{p,q-1}^{n}-\bar{R}_{p,q+1}^{n})\\
&\qquad+C_{13}(\bar{R}_{p,q-1}^{n}-2\bar{R}_{p,q}^{n}+\bar{R}_{p,q+1}^{n}),
\end{aligned} \tag{22}$$

where

$$C_1 = \frac{\Delta Y}{2\Delta X}, C_4 = C_9 = C_{14} = \frac{U^n_{p,q}\Delta\xi}{2\Delta X},$$
$$C_2 = C_7 = C_{12} = \frac{V^n_{p,q}\Delta\xi}{4\Delta Y}, C_8 = \frac{\Delta\xi}{2P_r(\Delta Y)^2},$$
$$C_3 = \frac{\Delta\xi}{2(\Delta Y)^2}, C_{13} = \frac{\Delta\xi}{2S_c(\Delta Y)^2}, \quad (23)$$
$$C_{10} = C_{11} = \frac{\phi\Delta\xi}{2},$$
$$C_5 = \left(\frac{\Delta\xi}{2}\right) G_r sin(\alpha), C_6 = \left(\frac{\Delta\xi}{2}\right) G_m,$$

and the initial and boundary values are as follows,

at $n = 0$

$U^0_{p,q} = 0,\ V^0_{p,q} = 0,\ \bar{W}^0_{p,q} = 0,\ \bar{R}^0_{p,q} = 0$ everywhere,

at $n > 0$

$$U^n_{0,q} = 0,\ V^n_{0,q} = 0,\ \bar{W}^n_{0,q} = 0,\ \bar{R}^n_{0,q} = 0,\ \text{at } p = 0,$$
$$U^n_{p,0} = 0,\ V^n_{p,0} = 0,\ \bar{W}^n_{p,0} = 1,\ \bar{R}^n_{p,0} = 1,\ \text{at } q = 0,$$
$$U^n_{p,N_y} = 0,\ V^n_{p,N_y} = 0,\ \bar{W}^n_{p,N_y} = 0,\ \bar{R}^n_{p,N_y} = 0,\ \text{at } y = N_y. \quad (24)$$

Then, we rewrite the finite difference of numerical scheme (19)-(23) as follows, so that the Thomas algorithm can be employed easily,

$$\begin{aligned} &A_1 U^{n+1}_{i,j-1} + B_1 U^{n+1}_{i,j} + R_1 U^{n+1}_{i,j+1} = E_1,\\ &A_2 \bar{W}^{n+1}_{i,j-1} + B_2 \bar{W}^{n+1}_{i,j} + R_2 \bar{W}^{n+1}_{i,j+1} = E_2,\\ &A_3 \bar{R}^{n+1}_{i,j-1} + B_3 \bar{R}^{n+1}_{i,j} + R_3 \bar{R}^{n+1}_{i,j+1} = E_3,\\ &V^{n+1}_{i,j} = E_4, \end{aligned} \quad (25)$$

where

$$A_1 = -C_2 - C_3, B_1 = 1 + C_4 + 2C_3,$$
$$R_1 = C_2 - C_3, A_2 = -C_7 - C_8,$$
$$B_2 = 1 + C_9 + 2C_8 + C_{10}, R_2 = C_7 - C_8,$$
$$A_3 = -C_{12} - C_{13}, B_3 = 1 + C_{14} + 2C_{13},$$
$$R_3 = C_{12} - C_{13},$$
$$E_4 = V^{n+1}_{p,q-1} - V^n_{p,q} + V^n_{p,q-1} - C_1 \begin{pmatrix} U^{n+1}_{p,q} - U^{n+1}_{p-1,q} + U^n_{p,q} - U^n_{p-1,q} + \\ U^{n+1}_{p,q-1} - U^{n+1}_{p-1,q-1} + U^n_{p,q-1} - U^n_{p-1,q-1} \end{pmatrix},$$
$$E_1 = U^n_{p,q} + C_4(U^{n+1}_{p-1,q} + U^n_{p-1,q} - U^n_{p,q}) + C_2(U^n_{p,q-1} - U^n_{p,q+1}) + C_3(U^n_{p,q-1} - 2U^n_{p,q} + U^n_{p,q+1}) + C_5(\bar{W}^{n+1}_{p,q} + \bar{W}^n_{p,q}) + C_6(\bar{R}^{n+1}_{p,q} + \bar{R}^n_{p,q}),$$
$$E_2 = (1 - C_{11})\bar{W}^n_{p,q} + C_9(\bar{W}^{n+1}_{p-1,q} + \bar{W}^n_{p-1,q} - \bar{W}^n_{p,q}) + C_7(\bar{W}^n_{p,q-1} - \bar{W}^n_{p,q+1}) + C_8(\bar{W}^n_{p,q-1} - 2\bar{W}^n_{p,q} + \bar{W}^n_{p,q+1}),$$
$$E_3 = \bar{R}^n_{p,q} + C_{14}(\bar{R}^{n+1}_{p-1,q} + \bar{R}^n_{p-1,q} - \bar{R}^n_{p,q}) + C_{12}(\bar{R}^n_{p,q-1} - \bar{R}^n_{p,q+1}) + C_{13}(\bar{R}^n_{p,q-1} - 2\bar{R}^n_{p,q} + \bar{R}^n_{p,q+1}).$$

The subscripts p and q represent the indexes in X-axis and Y-axis respectively. Meanwhile, the superscript n represents the index in time defined as $\xi = n\Delta\xi$, where $n = 0, 1, 2, \ldots, N_t$. Based on the initial conditions (12), the values of $U, V, \bar{W}, \bar{R}$ are given at $\xi = 0$. The first step of time at ξ, the coefficients $U_{p,q}$ and $V_{p,q}$ in finite difference approximations (14) and (13) are considered constant. The step of time at $\xi = 1, 2, ..., N_t$, the temperature T^{n+1}, concentration C^{n+1}, velocity along plate U^{n+1} are solved by using Thomas algorithm and the velocity in normal to plate V^{n+1} is solved iteratively in equations (19)-(23) at all nodes of grid in space. This step is repeated until the interation of time achieves at the final step N_t. The values $U, V, \bar{W}, \bar{R}$ in (19)-(23) should become smaller and smaller while time t approaches to the final step N_t.

The equations $(25)_1$, $(25)_2$ and $(25)_3$ are solved numerically by using Thomas algorithm, and the equation $(25)_4$ is only solved iteratively. Then, we present the equations $(25)_1$, $(25)_2$ and $(25)_3$ as the tri-diagonal matrices, for $p = 0, 1, 2, ..., N_x$ and $q = 0, 1, 2, ..., N_y$.

$$\begin{bmatrix} B_1 & R_1 & 0 & 0 & \cdots & 0 \\ A_1 & B_1 & R_1 & 0 & \cdots & 0 \\ 0 & A_1 & B_1 & \ddots & \cdots & \vdots \\ 0 & 0 & \ddots & \ddots & R_1 & 0 \\ \vdots & \vdots & \vdots & A_1 & B_1 & R_1 \\ 0 & 0 & \cdots & 0 & A_1 & B_1 \end{bmatrix} \begin{bmatrix} U^{n+1}_{p,1} \\ U^{n+1}_{p,2} \\ U^{n+1}_{p,3} \\ \vdots \\ U^{n+1}_{p,N_y-2} \\ U^{n+1}_{p,N_y-1} \end{bmatrix} = \begin{bmatrix} E_1 \\ E_1 \\ E_1 \\ \vdots \\ E_1 \\ E_1 \end{bmatrix} + \begin{bmatrix} U^{n+1}_{p,0} \\ 0 \\ 0 \\ \vdots \\ 0 \\ U^{n+1}_{p,N_y} \end{bmatrix}. \quad (26)$$

$$\begin{bmatrix} B_2 & R_2 & 0 & 0 & \cdots & 0 \\ A_2 & B_2 & R_2 & 0 & \cdots & 0 \\ 0 & A_2 & B_2 & \ddots & \cdots & \vdots \\ 0 & 0 & \ddots & \ddots & R_2 & 0 \\ \vdots & \vdots & \vdots & A_2 & B_2 & R_2 \\ 0 & 0 & \cdots & 0 & A_2 & B_2 \end{bmatrix} \begin{bmatrix} \bar{W}^{n+1}_{p,1} \\ \bar{W}^{n+1}_{p,2} \\ \bar{W}^{n+1}_{p,3} \\ \vdots \\ \bar{W}^{n+1}_{p,N_y-2} \\ \bar{W}^{n+1}_{p,N_y-1} \end{bmatrix} = \begin{bmatrix} E_2 \\ E_2 \\ E_2 \\ \vdots \\ E_2 \\ E_2 \end{bmatrix} + \begin{bmatrix} \bar{W}^{n+1}_{p,0} \\ 0 \\ 0 \\ \vdots \\ 0 \\ \bar{W}^{n+1}_{p,N_y} \end{bmatrix}. \quad (27)$$

$$\begin{bmatrix} B_3 & R_3 & 0 & 0 & \cdots & 0 \\ A_3 & B_3 & R_3 & 0 & \cdots & 0 \\ 0 & A_3 & B_3 & \ddots & \cdots & \vdots \\ 0 & 0 & \ddots & \ddots & R_3 & 0 \\ \vdots & \vdots & \vdots & A_3 & B_3 & R_3 \\ 0 & 0 & \cdots & 0 & A_3 & B_3 \end{bmatrix} \begin{bmatrix} \bar{R}^{n+1}_{p,1} \\ \bar{R}^{n+1}_{p,2} \\ \bar{R}^{n+1}_{p,3} \\ \vdots \\ \bar{R}^{n+1}_{p,N_y-2} \\ \bar{R}^{n+1}_{p,N_y-1} \end{bmatrix} = \begin{bmatrix} E_3 \\ E_3 \\ E_3 \\ \vdots \\ E_3 \\ E_3 \end{bmatrix} + \begin{bmatrix} \bar{R}^{n+1}_{p,0} \\ 0 \\ 0 \\ \vdots \\ 0 \\ \bar{R}^{n+1}_{p,N_y} \end{bmatrix}. \quad (28)$$

The previous results of tri-diagonal matrices (26), (27) and (28) are represented as the following tri-diagonal matrix

$$\begin{bmatrix} \psi_1 & c_1 & 0 & 0 & \cdots & 0 \\ \Phi_2 & \psi_2 & c_2 & 0 & \cdots & 0 \\ 0 & \Phi_3 & \psi_3 & \ddots & \cdots & \vdots \\ 0 & 0 & \ddots & \ddots & c_{N-2} & 0 \\ \vdots & \vdots & \vdots & \Phi_{N-1} & \psi_{N-1} & c_{N-1} \\ 0 & 0 & \cdots & 0 & \Phi_N & \psi_N \end{bmatrix} \begin{bmatrix} v_1 \\ v_2 \\ v_3 \\ \vdots \\ v_{N-1} \\ v_N \end{bmatrix} = \begin{bmatrix} d_1 \\ d_2 \\ d_3 \\ \vdots \\ d_{N-1} \\ d_N \end{bmatrix}$$

, which gives the following two-diagonal matrix

$$\begin{bmatrix} \psi_1^{'} & c_1 & 0 & 0 & \cdots & 0 \\ 0 & \psi_2^{'} & c_2 & 0 & \cdots & 0 \\ 0 & 0 & \psi_3^{'} & \ddots & \cdots & \vdots \\ 0 & 0 & \ddots & \ddots & c_{N-2} & 0 \\ \vdots & \vdots & \vdots & 0 & \psi_{N-1}^{'} & c_{N-1} \\ 0 & 0 & \cdots & 0 & 0 & \psi_N^{'} \end{bmatrix} \begin{bmatrix} v_1 \\ v_2 \\ v_3 \\ \vdots \\ v_{N-1} \\ v_N \end{bmatrix} = \begin{bmatrix} d_1^{'} \\ d_2^{'} \\ d_3^{'} \\ \vdots \\ d_{N-1}^{'} \\ d_N^{'} \end{bmatrix}.$$

The above two-diagonal matrix can be solved iteratively by applying the following formula

$$\psi_1^{'} = \psi_1,\ d_1^{'} = d_1,\ \psi_i^{'} = \psi_i - c_{i-1}\frac{\Phi_i}{\psi_{i-1}^{'}},$$
$$d_i^{'} = d_i - d_{i-1}^{'}\frac{\Phi_i}{\psi_{i-1}^{'}},\ \text{for } i = 2, 3, ..., N,$$

and

$$v(N) = \frac{d^{'}(N)}{\psi^{'}(N)},\ v(i) = \frac{d^{'}(i) - c(i)v(i+1)}{\psi^{'}(i)},$$
$$\text{for } i = N-1, N-2, ..., 2, 1.$$

Then the profiles of velocity U, temperature $\bar{W}$, and concentration $\bar{R}$ for different values of Prandtl number (P_r), Grashof number (G_r), Modified Grashof number (G_m), Schmidt number (S_c) are obtained based on the finite difference approximations. Figures 3, 9, and 15 establish the same velocity profiles for different Grashof (G_r), modified Grashof (G_m), and inclination angle (α). The velocity profiles are more increased when Grashof, modified Grashof, and and inclination angle are more increased. Meanwhile, the velocity profiles are more decreased when Prandtl (P_r) and Schmidt (S_c) are more increased in Figure 6 and Figure 12. The increase of velocity profile for increased inclination angle makes sense because when the fluid moves along the inclined flat plate, it will require more force for fluid to pass through the inclined flat plate. We also observe that the temperature profiles are decreased with the increases of Grashof (G_r), (P_r), modified Grashof (G_m), and inclination angle (α) from Figures 4, 7, 10, and 16 respectively. The temperature is more increased while the increases of Schmidt number for different Schmidt (S_c). Figures 5, 11, 14, and 17 show that the concentration profiles decrease with the increases of Grashof (G_r), modified Grashof (G_m), Schmidt (S_c), and inclination angle (α). The concentration profile increases when Prandtl (P_r) are more increased as in Figure 8. Figures 15, 16, 17 are respectively the velocity, temperature, and concentration profiles when the angle of inclination $\alpha = 45^0$ (solid line) and $\alpha = 90^0$ (dotted line). The velocity profile for inclined flat plate ($\alpha = 45^0$) is more sloping than ($\alpha = 90^0$). This result makes sense because when the fluid moves along the inclined flat plate with the higher angle inclination, it will require more force (causing more velocity) for fluid to pass through the inclined flat plate. Meanwhile, the temperature and concentration profiles over inclined flat plate between ($\alpha = 45^0$) and ($\alpha = 90^0$), there is no significant difference because the angle of inclination does not affect the temperature and concentration of fluid passing through the inclined flat plate.

IV. Stability Analysis

We are now concerned with the stability of the finite difference scheme. Let assume that the forms $e^{i\beta p\Delta X}$ and $e^{i\beta q\Delta Y}$ are general term of fourier expansion for $U, \bar{W}$ and $\bar{R}$ at time $\xi = 0$. Then, these terms can be written more general as follows at $\xi > 0$,

$$\begin{aligned} U &= K(\xi)e^{i\beta p\Delta X}e^{i\beta q\Delta Y}, \\ \bar{W} &= L(\xi)e^{i\beta p\Delta X}e^{i\beta q\Delta Y}, \\ \bar{R} &= M(\xi)e^{i\beta p\Delta X}e^{i\beta q\Delta Y}. \end{aligned} \tag{29}$$

The values of $K(\xi)$, $L(\xi)$, and $M(\xi)$ at one step of time are denoted respectively by K', L', and M'. Substituting (29) into (18)-(17), and dividing the results by $e^{i\beta p\Delta X}$ and $e^{i\beta q\Delta Y}$, then one has

$$\begin{aligned} &\frac{K'-K}{\Delta\xi} + \frac{U}{2\Delta X}(K'+K)(1-e^{-i\beta\Delta X}) \\ &+ \frac{V}{2\Delta Y}(K'+K)i\ sin(\beta\Delta Y) \\ &= \frac{1}{(\Delta Y)^2}(K'+K)(cos(\beta\Delta Y)-1) \\ &\quad + \frac{G_r}{2}(L'+L)sin(\alpha) + \frac{G_m}{2}(M'+M), \end{aligned} \tag{30}$$

$$\begin{aligned} &\frac{L'-L}{\Delta\xi} + \frac{U}{2\Delta X}(L'+L)(1-e^{-i\beta\Delta X}) \\ &+ \frac{V}{2\Delta Y}(L'+L)i\ sin(\beta\Delta Y) \\ &= \frac{1}{P_r(\Delta Y)^2}(L'+L)(cos(\beta\Delta Y)-1) - \frac{\phi}{2}(L'+L), \end{aligned} \tag{31}$$

$$\begin{aligned} &\frac{M'-M}{\Delta\xi} + \frac{U}{2\Delta X}(M'+M)(1-e^{-i\beta\Delta X}) \\ &+ \frac{V}{2\Delta Y}(M'+M)i\ sin(\beta\Delta Y) \\ &= \frac{1}{2S_c(\Delta Y)^2}(M'+M)(cos(\beta\Delta Y)-1). \end{aligned} \tag{32}$$

Let us define that

$$\begin{aligned} A &= \frac{\Delta\xi U}{2\Delta X}(1-e^{-i\beta\Delta X}) + \frac{\Delta\xi V}{2\Delta Y}i\ sin(\beta\Delta Y) \\ &\quad - \frac{\Delta\xi}{(\Delta Y)^2}(cos(\beta\Delta Y)-1), \\ B &= \frac{\Delta\xi U}{2\Delta X}(1-e^{-i\beta\Delta X}) + \frac{\Delta\xi V}{2\Delta Y}i\ sin(\beta\Delta Y) \\ &\quad - \frac{\Delta\xi}{P_r(\Delta Y)^2}(cos(\beta\Delta Y)-1), \\ C &= \frac{\Delta\xi U}{2\Delta X}(1-e^{-i\beta\Delta X}) + \frac{\Delta\xi V}{2\Delta Y}i\ sin(\beta\Delta Y) \\ &\quad - \frac{\Delta\xi}{2S_c(\Delta Y)^2}(cos(\beta\Delta Y)-1). \end{aligned} \tag{33}$$

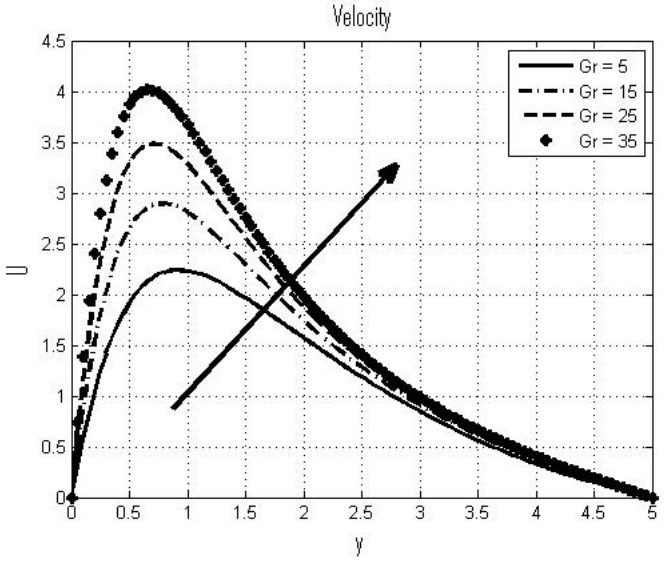

Fig. 3. Velocity profile for various Grashof number

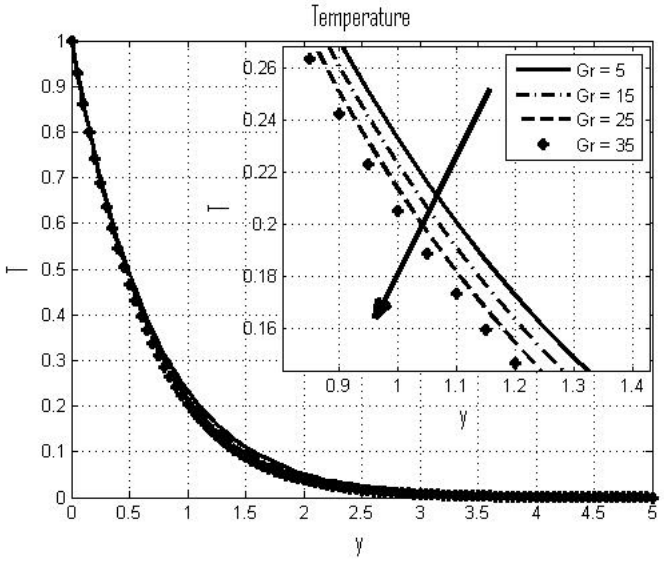

Fig. 4. Temperature profile for various Grashof number

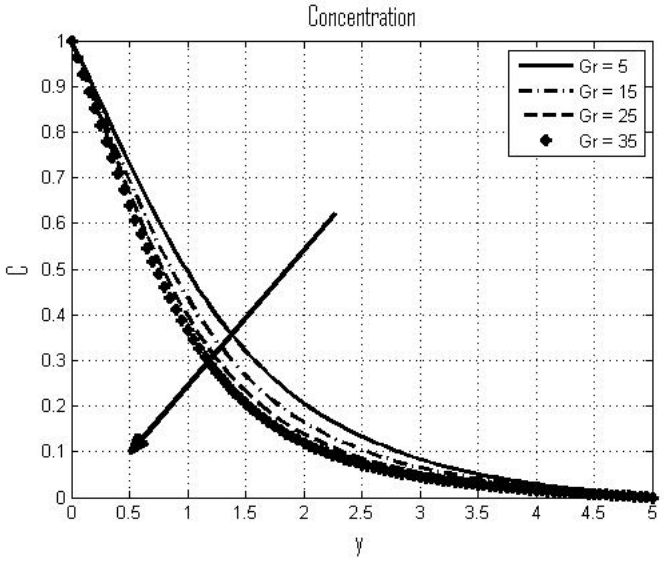

Fig. 5. Concentration profile for various Grashof number

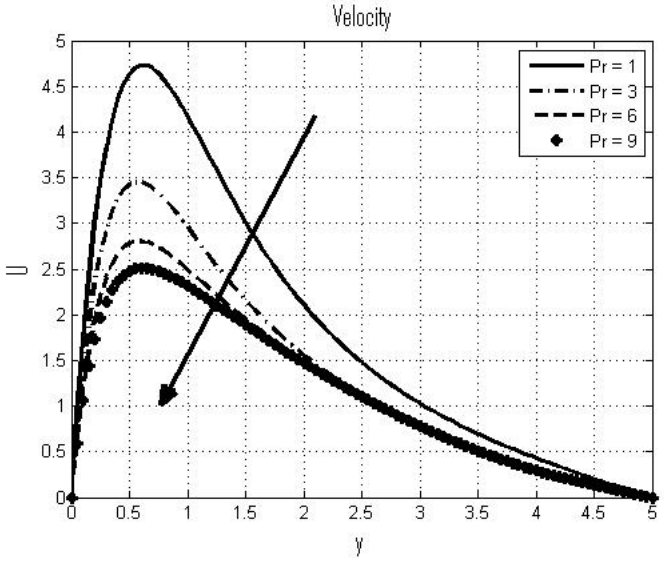

Fig. 6. Velocity profile for various Prandtl number

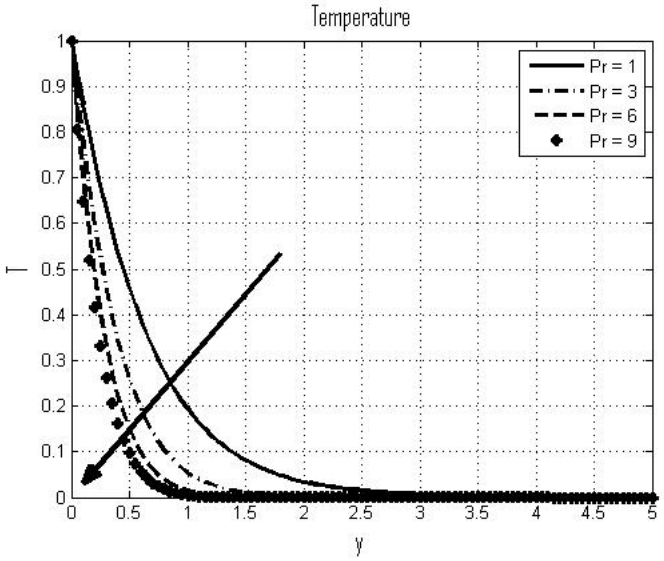

Fig. 7. Temperature profile for various Prandtl number

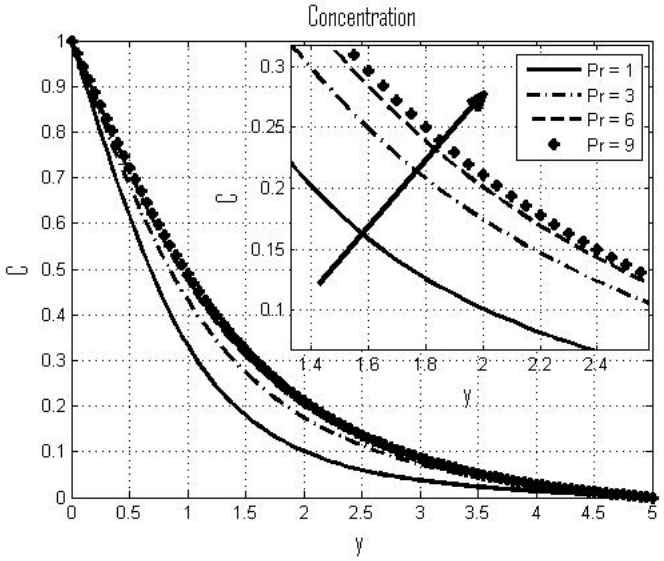

Fig. 8. Concentration profile for various Prandtl number

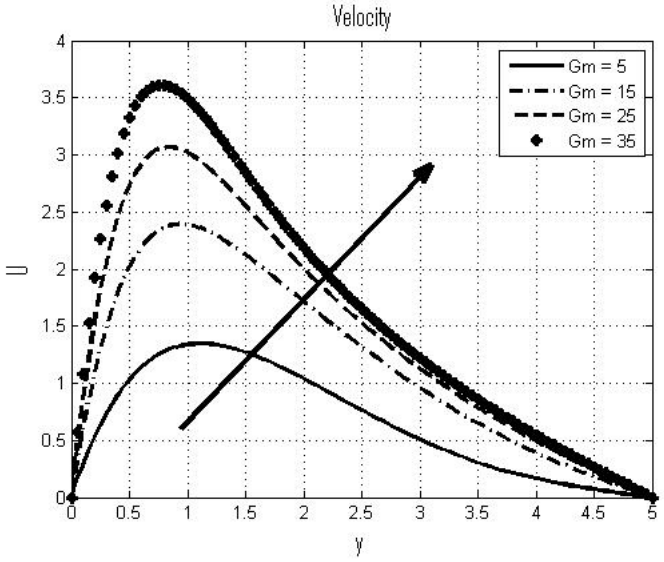

Fig. 9. Velocity profile for various Modified Grashof number

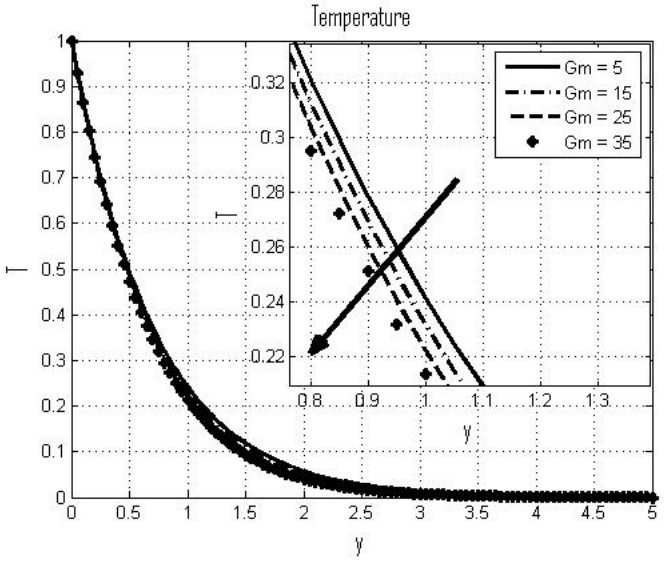

Fig. 10. Temperature profile for various Modified Grashof number

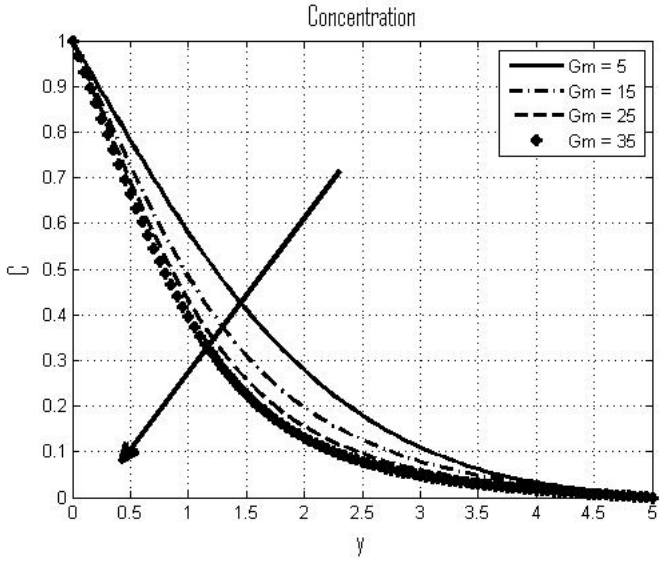

Fig. 11. Concentration profile for various Modified Grashof number

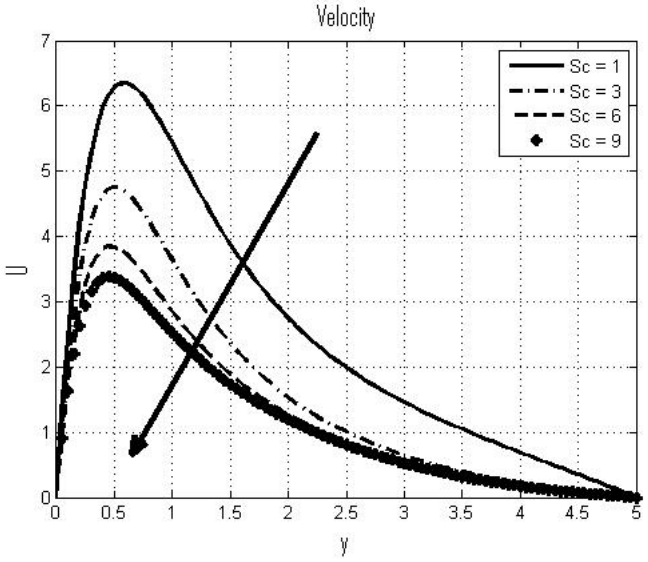

Fig. 12. Velocity profile for various Schmidt number

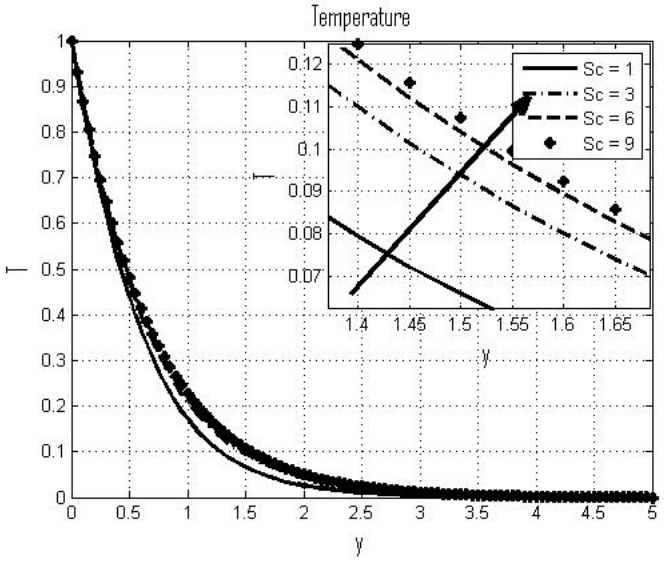

Fig. 13. Temperature profile for various Schmidt number

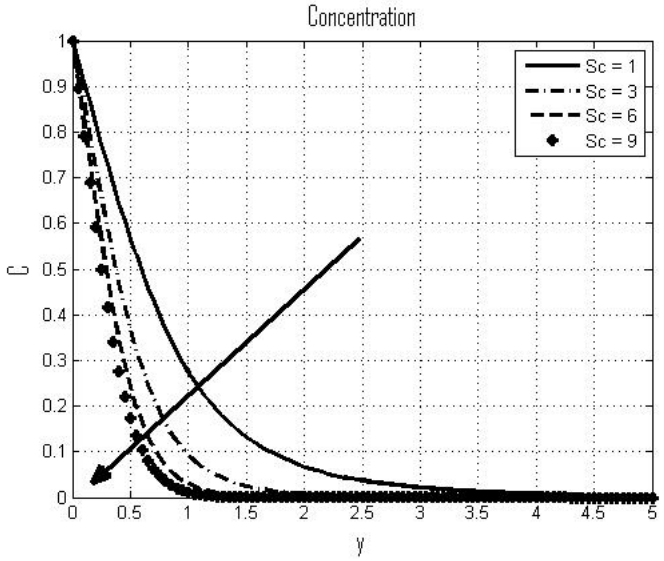

Fig. 14. Concentration profile for various Schmidt number

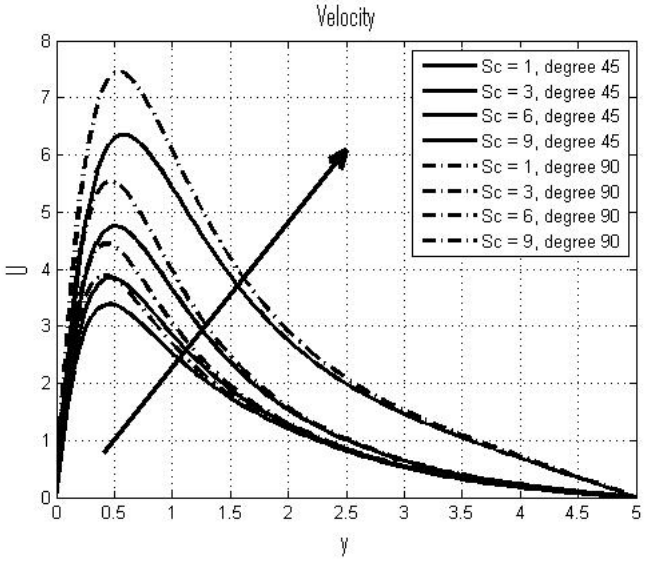

Fig. 15. Velocity profile for various inclination angle

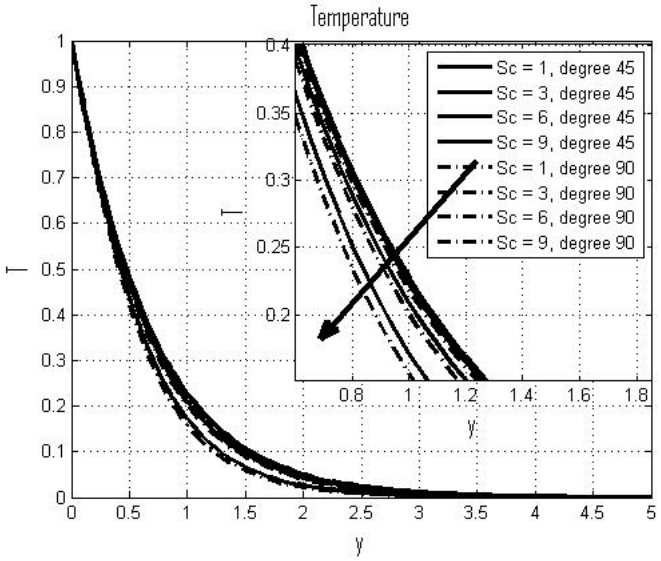

Fig. 16. Temperature profile for various inclination angle

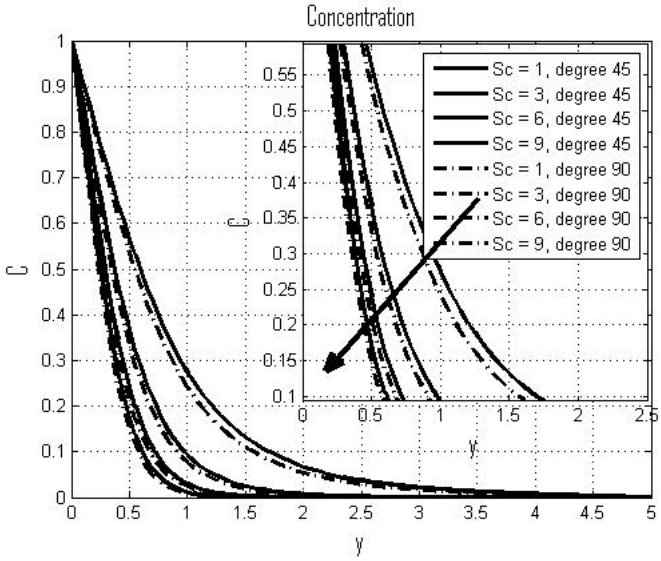

Fig. 17. Concentration profile for various inclination angle

Then (30)-(32) becomes

$$(1+A)K' = (1-A)K + \frac{\Delta\xi G_r}{2}(L'+L)sin(\alpha) + \frac{\Delta\xi G_m}{2}(M'+M). \quad (34)$$

$$(1+B)L' = (1-B)L \Rightarrow L' = \left(\frac{1-B}{1+B}\right)L. \quad (35)$$

$$(1+C)M' = (1-C)M \Rightarrow M' = \left(\frac{1-C}{1+C}\right)M. \quad (36)$$

Substituting (35)-(36) into (34) to get

$$K' = \left(\frac{1-A}{1+A}\right)K + \frac{\Delta\xi G_r sin(\alpha)}{(1+A)(1+B)}L + \frac{\Delta\xi G_m}{(1+A)(1+C)}M, \quad (37)$$

which can be represented as the following matrix

$$\begin{bmatrix} K' \\ L' \\ M' \end{bmatrix} = \begin{bmatrix} a_{11} & a_{12} & a_{13} \\ 0 & a_{22} & 0 \\ 0 & 0 & a_{33} \end{bmatrix} \begin{bmatrix} K \\ L \\ M \end{bmatrix}, \quad (38)$$

where

$$a_{11} = \left(\frac{1-A}{1+A}\right),\ a_{12} = \frac{\Delta\xi G_r sin(\alpha)}{(1+A)(1+B)},$$
$$a_{13} = \frac{\Delta\xi G_m}{(1+A)(1+C)},\ a_{22} = \left(\frac{1-B}{1+B}\right),\ a_{33} = \left(\frac{1-C}{1+C}\right).$$

It follows from (38), one can find the eigen values

$$\lambda_1 = \left(\frac{1-A}{1+A}\right), \lambda_2 = \left(\frac{1-B}{1+B}\right),\ \lambda_3 = \left(\frac{1-C}{1+C}\right),$$

and also from (33), one has

$$A = \frac{\Delta\xi U}{\Delta X}sin^2\left(\frac{\beta\Delta X}{2}\right) + \frac{2\Delta\xi V}{\Delta Y}sin^2\left(\frac{\beta\Delta Y}{2}\right) + i\frac{\Delta\xi U}{2\Delta X}sin(\beta\Delta X),$$

$$B = \frac{\Delta\xi U}{\Delta X}sin^2\left(\frac{\beta\Delta X}{2}\right) + \frac{2\Delta\xi V}{P_r\Delta Y}sin^2\left(\frac{\beta\Delta Y}{2}\right) + i\frac{\Delta\xi U}{2\Delta X}sin(\beta\Delta X),$$

$$C = \frac{\Delta\xi U}{\Delta X}sin^2\left(\frac{\beta\Delta X}{2}\right) + \frac{2\Delta\xi V}{S_c\Delta Y}sin^2\left(\frac{\beta\Delta Y}{2}\right) + i\frac{\Delta\xi U}{2\Delta X}sin(\beta\Delta X).$$

Since $0 < sin\left(\frac{\beta\Delta X}{2}\right), sin\left(\frac{\beta\Delta Y}{2}\right), sin(\beta\Delta X) < 1$, then $A, B, C > 0$ which gives the eigen values $\lambda_{1,2,3} < 0$. Hence, the Crank-Nicolson is unconditionally stable.

V. Conclusions

We can make the following summaries for velocity, temperature, and concentration profiles based on the results and discussions for the problem of natural convection flow over an inclined flat plate.

1) When Grashof and modified Grashof are increased, the velocity profiles increase. Meanwhile, the velocity profiles are more decreased when Prandtl (P_r) and Schmidt (S_c) are more decreased.
2) The temperature profiles are decreased with the increases of Grashof (G_r), Prandtl (P_r), and modified Grashof (G_m). Moreover, the temperature is more increased while the increases of Schmidt number for different Schmidt (S_c).
3) The concentration profiles decrease with the increases of Grashof (G_r), modified Grashof (G_m), and Schmidt (S_c). The concentration profile increases when Prandtl (P_r) are more increased.
4) The velocity profile for inclined flat plate ($\alpha = 45^0$) is more sloping than ($\alpha = 90^0$). This result makes sense because when the fluid moves along the inclined flat plate, it will require more force for fluid to pass through the inclined flat plate. Meanwhile, the temperature and concentration profiles over an inclined flat plate between ($\alpha = 45^0$) and ($\alpha = 90^0$) are studied. Because the angle of inclination has no effect on the temperature and concentration of fluid passing through the inclined flat plate, there is no significant difference.
5) The Crank-Nicolson scheme is unconditionally stable when the general term of Fourier expansion is used for stability calculations.

References

[1] N. Amin, R. Nazar, and I. Pop, "On the mixed convection boundary-layer flow about a solid sphere with constant surface temperature," Arabian Journal for Science and Engineering. 27 (2), 117-135, 2002.

[2] Y. S. Daniel, Z. A. Aziz, Z. Ismail, and F. Salah, "Slip Effects on Electrical Unsteady MHD Natural Convection Flow of Nanofluid over a Permeable Shrinking Sheet with Thermal Radiation," Engineering Letter 26, no. 1, 107-116, 2018.

[3] K. Gangadhar, D. Vijayakumar, A. J. Chamkha, T. Kannan, and G. Sakthivel, "Effects of Newtonian heating and thermal radiation on micropolar ferrofluid flow past a stretching surface: spectral quasi-linearization method," Heat Transfer 49, no. 2, 838-857, 2020.

[4] M. Ghani, B. Widodo, and C. Imron, "Incompressible and steady mixed convection flow over a sphere," The 1st Young Scientist International Conference of Water Resources Development and Environmental Protection, Malang, Indonesia, 2015.

[5] M. Ghani and W. Rumite, "Keller-Box scheme to mixed convection flow over a solid sphere with the effect of MHD," MUST: Journal of Mathematics Education, Science and Technology. 6 (1), 97-120, 2021.

[6] M. Ghani, "Numerical results of mixed convection flow over a flat plate with the imposed heat and inclination angle," Euler: Jurnal Ilmiah Matematika, Sains, dan Teknologi. 9(2), 85-93, 2021.

[7] Md. Islam, Md. Samsuzzoha, S. Ara, N. Islam, "Unsteady Solutions of Thermal Boundary Layer Equations by using Finite Difference Method," Annals of Pure and Applied Mathematics. 3(2), 142-154, 2013.

[8] R. Jusoh, R. Nazar, and I. Pop, "Magnetohydrodynamic rotating flow and heat transfer of ferrofluid due to an exponentially permeable stretching/shrinking sheet," Journal of Magnetism and Magnetic Materials 465, 365-374, 2018.

[9] A. R. M. Kasim, "Convective boundary layer of viscoelastic fluid," Ph.D. Thesis. Malaysia: Universiti Teknologi Malaysia, 2014.

[10] W. A. Khan, Z. H. Khan, and R. Ul Haq, "Flow and heat transfer of ferrofluids over a flat plate with uniform heat flux," The European Physical Journal Plus 130, no. 4, 1-10, 2015.

[11] K. A. Kumar, K. Anantha, N. Sandeep, V. Sugunamma, and I. L. Animasaun, "Effect of irregular heat source/sink on the radiative thin film flow of MHD hybrid ferrofluid," Journal of Thermal Analysis and Calorimetry 139, no. 3, 2145-2153, 2020.

[12] G. Makanda, S. Shaw, and P. Sibanda, "Effects of radiation on MHD free convection of a Casson fluid from a horizontal circular cylinder with partial slip in non-Darcy porous medium with viscous dissipation," Boundary Value Problems 2015, no. 1, 1-14, 2015.

[13] M. K. A. Mohamed, N. A. Ismail, N. Hashim, N. M. Shah, and M. Z. Salleh, "MHD slip flow and heat transfer on stagnation point of a magnetite (Fe3O4) ferrofluid towards a stretching sheet with Newtonian heating," CFD Letters 11, no. 1, 17-27, 2019.

[14] I. Nayak, "Numerical Study of MHD Flow and Heat Transfer of an Unsteady Third Grade Fluid with Viscous Dissipation," IAENG International Journal of Applied Mathematics, 49, no.2, 245-252, 2019.

[15] R. Nazar, I. Pop, and M. Z. Salleh, “Mixed convection boundary layer flow about a solid sphere with newtonian heating,” Archives of Mechanics. 62(4), 283-303, 2010.
[16] A. A. Opanuga, S. O. Adesanya, S. A. Bishop, H. I. Okagbue, and O. O. Agboola, ”Entropy Generation of Unsteady MHD Couette Flow through Vertical Microchannel with Hall and Ion Slip Effects,” IAENG International Journal of Applied Mathematics, 50, no.3, 666-677, 2020.
[17] A. M. Rashad, ”Impact of anisotropic slip on transient three dimensional MHD flow of ferrofluid over an inclined radiate stretching surface,” Journal of the Egyptian Mathematical Society 25, no. 2, 230-237, 2017.
[18] F. Salah, Z. A. Aziz, and D. L. C. Ching, ” On Accelerated MHD Flows of Second Grade Fluid in a Porous Medium and Rotating Frame,” IAENG International Journal of Applied Mathematics, 43, no.3, 106-113, 2013.
[19] B. Widodo, I. Anggriani, D. A. Khalimah, and F. D. S. Zainal, “Unsteady Boundary Layer Magnetohydrodynamics in Micropolar Fluid Past A Sphere,” Far East Journal of Mathematical Sciences. 100, 291-299, 2016.
[20] S. H. M. Yasin, M. K. A. Mohamed, Z. Ismail, and M. Z. Salleh, ”Mathematical solution on MHD stagnation point flow of ferrofluid,” In Defect and Diffusion Forum, vol. 399, pp. 38-54. Trans Tech Publications Ltd, 2020.
[21] A. Zeeshan, A. Majeed, and R. Ellahi, ”Effect of magnetic dipole on viscous ferro-fluid past a stretching surface with thermal radiation,” Journal of Molecular Liquids 215, 549-554, 2016.